

Thermal behavior, decomposition mechanism and thermal safety of 5,7-diamino-4,6-dinitrobenzenefuroxan (CL-14)

Xiao-Long Fu¹ · Xue-Zhong Fan¹ · Bo-Zhou Wang¹ · Huan Huo¹ ·
Ji-Zhen Li¹ · Rong-Zu Hu¹

Received: 20 March 2015 / Accepted: 16 August 2015
© Akadémiai Kiadó, Budapest, Hungary 2015

Abstract Thermal decomposition kinetics and mechanism of the high-energetic material 5,7-diamino-4,6-dinitrobenzenefuroxan (CL-14) were determined by differential scanning calorimetry (DSC), rapid scanning Fourier transform infrared spectroscopy, and simultaneous thermogravimetric and DSC analyses, coupled with FT-IR and mass spectroscopy. To evaluate the thermal safety of 5,7-diamino-4,6-dinitrobenzenefuroxan (CL-14), its specific heat capacity (C_p) was measured by DSC, and thermal conductivity (λ) was estimated. Kinetic parameters and heat of exothermic decomposition reaction of CL-14 were obtained by analysis of DSC curves. Kinetic parameters used to evaluate the thermal safety of CL-14, such as self-accelerating decomposition temperature (T_{SADT}), critical temperature of thermal explosion (T_b) and impact sensitivity (H_{50}), were obtained. Results showed that for CL-14, $T_{SADT} = 282.0$ °C and $T_b = 307.9$ °C, whereas $H_{50} = 39.79$ cm, revealing that CL-14 had better thermal safety and heat resistance than HMX, RDX and GNTO.

Keywords Applied chemistry · 5,7-Diamino-4,6-dinitrobenzenefuroxan · Thermal decomposition · Thermal safety · RSFT-IR · TG-DSC-MS-FT-IR

Introduction

Benzenefuroxan has attracted attention as high-energetic materials (HEMs) because of its structural peculiarities and high densities [1–4]. The densities of explosive molecules and velocity of detonation can be increased when nitro groups were replaced with furoxan groups [5–7]. Meanwhile, the introduction of amino groups to explosive molecules can further enhance heat resistance and density, as well as decrease impact sensitivity [8–11]. In view of improvements in thermal stability and insensitivity, 5,7-diamino-4,6-dinitrobenzenefuroxan (CL-14) has been studied as substitute for several traditional energetic materials, such as 1,3,5-triamino-2,4,6-trinitrobenzene (TATB), cyclotrimethylene trinitramine (RDX) and cyclotetramethylene tetranitramine (HMX) [12]. CL-14 can be used as HEMs in propellants, explosives and gun powders because of its high density, appropriate detonation velocity and low sensitivity [13, 14]. The synthesis of CL-14 was reported in the literature [15]. The melting point and mechanical properties of CL-14-based PBXs were investigated [12]. In addition, the salts of CL-14 were synthesized, and the mechanical sensitivities of the salts were tested [16].

Modern ordinance dictates strong requirements for HEMs with low impact and shock insensitivity, good thermal stability and better performance [17–20]. Among the study methods of HEMs, thermal analysis study is important not only for understanding of the kinetics of their thermal decomposition but also for assessing the effect of their exothermic decomposition on the potential hazardous in their processing, handling and storage [21–23]. Kinetic studies also provide useful information on thermal stability of HEMs under different thermal environment in storage [24–26]. However, the kinetics and mechanism of the

✉ Xiao-Long Fu
fuxiaolong204@163.com

¹ Xi'an Modern Chemistry Research Institute, Xi'an 710065, China

decomposition and the decomposition products of CL-14 are not documented.

In this work, the thermal behaviors, decomposition kinetics and mechanism as well as thermal safety of CL-14 have been experimentally investigated by several state-of-the-art techniques, such as differential scanning calorimetry (DSC) and thermogravimetric analyzer (TGA). Using the original DSC data, the critical temperature of thermal explosion (T_b), self-accelerating decomposition temperature (T_{SADT}) and the impact sensitivity (H_{50}) were estimated. Thus, the thermal safety of CL-14 was evaluated, which is useful for evaluating the process of the explosion from the thermal decomposition.

Experimental

Materials

CL-14 prepared by our work group is a yellow powder with >99.5 % purity. The synthesis of CL-14 is shown in Scheme 1. The structure and composition of CL-14 are as follows.

NMR spectra were recorded on a Bruker 500-MHz NMR spectrometer using DMSO- d_6 , as the solvent with tetramethylsilane as the internal standard. Elemental analysis was performed by PE-2400 instrument.

^1H NMR(DMSO- d_6 , 500 MHz, δ , ppm): 10.01(d, $J = 7.5$ Hz, 2H, NH_2), 10.85(d, $J = 5.0$ Hz, 2H, NH_2).

^{13}C NMR(DMSO- d_6 , 125 MHz, δ , ppm): 150.52(1C), 146.60(1C), 143.91(1C), 115.26(1C), 106.91(1C), 105.68(1C).
Anal. calcd for $\text{C}_6\text{H}_4\text{O}_6\text{N}_6$ (%): C 28.13, H 1.563, N 32.81.

Found C 28.37, H 1.617, N 32.54.

Equipment and experimentation

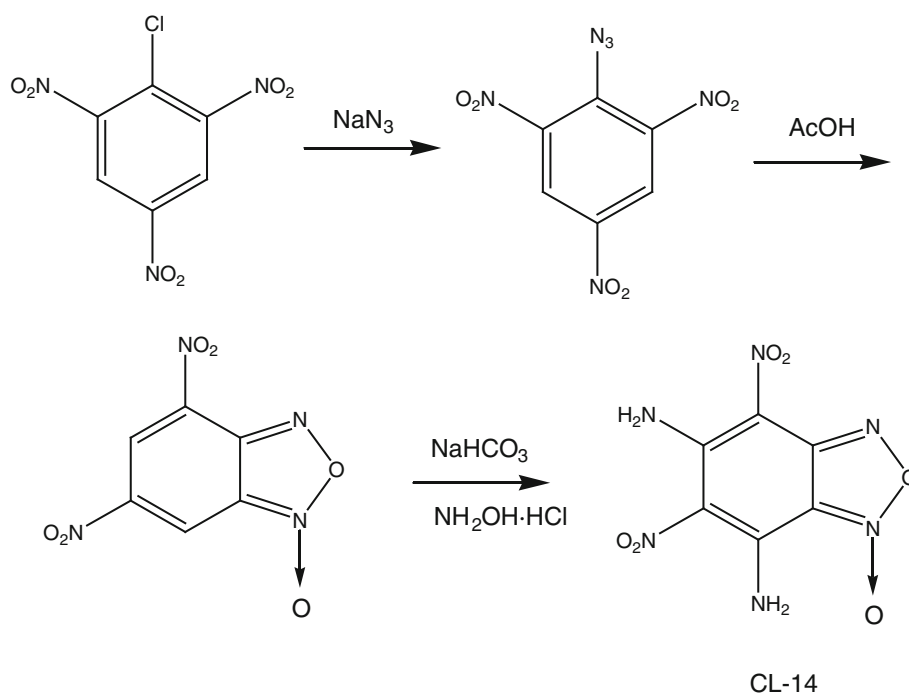
Differential scanning calorimetry (DSC)

The DSC experiments for CL-14 were performed by using a Model 910S DSC instrument (TA, USA). The CL-14 sample was placed in aluminum pans. Dry, oxygen-free nitrogen was used to purge the DSC at a rate of 50 mL min^{-1} . The heating rates were 5, 10, 15 and $20 \text{ }^\circ\text{C min}^{-1}$ from ambient temperature to $360 \text{ }^\circ\text{C}$, using a sample mass of 2.5 mg.

TG-DSC-MS-FT-IR

Thermogravimetric and differential scanning calorimetry (TG-DSC) TG-DSC curves were obtained using the Model 449C TG-DSC Instrument (Netzsch, Inc., Germany). The thermal decomposition experiment was conducted in the range of $35\text{--}380 \text{ }^\circ\text{C}$, with a heating rate of $10 \text{ }^\circ\text{C min}^{-1}$, and under a nitrogen atmosphere (flow rate of 75 L min^{-1}). TG and DSC curves obtained under the same conditions overlapped with each other, indicating that the reproducibility of the tests was satisfactory.

Scheme 1 The preparation route of CL-14



Fourier transform infrared spectroscopy (FT-IR) FT-IR spectra were carried out on a FT-IR spectrometer (Nicolet 5700, USA) operating in absorption mode over the frequency range of 4000–400 cm^{-1} . The temperature of the transfer line was maintained in the range from ambient temperature to 380 °C.

Mass spectroscopy analysis (MS) Mass spectra were recorded using a Quadruple Mass Spectrometer (Netzsch QMS403, Germany). The evolved gases during thermal decomposition experiments were directly transferred by means of a transfer line (heated to 380 °C) and detected by mass spectrometer.

Rapid scanning Fourier transform infrared spectroscopy (RSFT-IR)

RSFT-IR measurements were detected using a model NEXUS 870 FT-IR spectrophotometer (Nicolet Instruments Co., USA) and an in situ thermolysis cell (Xiamen University, China) within the temperature range of 20–465 °C and at a heating rate of 10 °C min^{-1} with a KBr pellet sample (about 0.7 mg of CL-14 and 150 mg of KBr). The IR spectra of CL-14 in the range of 4000–400 cm^{-1} were acquired by a model DTGS detector at a rate of 7.5 files min^{-1} and 8 scans file^{-1} with a resolution of 4 cm^{-1} .

Melting point instrument

The melting point (T_m) of CL-14 was measured by WRS-1B digital melting point instrument. The sample was dried at 50 °C for 10 h and filled into the capillary glass tube. The height of the sample was less than 3 mm. The heating rate was 1.5 °C min^{-1} . The melting point of CL-14 was determined to be 216.5 °C (489.5 K).

The specific heat capacity

The specific heat capacity (C_p) of CL-14 was determined by using the continuous mode of the DSC apparatus in the temperature range of 10–75 °C [24]. The standard molar heat capacity of CL-14 was 1.14 $\text{J mol}^{-1} \text{K}^{-1}$ at 298.15 K.

Results and discussion

Thermal behavior

The typical TG-DSC curves of CL-14 over the temperature range of 35–500 °C are shown in Fig. 1. From TG-DSC curve, only one sharp exothermic peak is observed in the DSC curve at approximately 301.4 °C, which corresponds to one-step mass loss of about 81 %. This exothermic

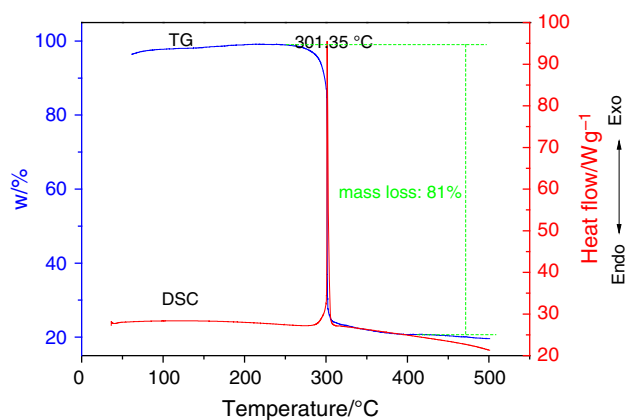


Fig. 1 TG-DSC curve of CL-14 by TG-DSC-MS-FT-IR

temperature was reported to be 308.5 °C in the literature [27] and may be caused by differences in the instrument setup and experimental conditions.

Figure 2 shows the DSC curves of CL-14 at several heating rates. We found that the decomposition temperature of CL-14 shifted to higher temperatures with the increase in heating rate. The shifts in onset temperature, peak temperature and end temperature are listed in Table 1. Interestingly, the heat of decomposition derived from the exothermic peak area increased with heating rate. These data are also listed in Table 1 and compared with those of HMX. Only one decomposition process of CL-14 was indicated by TG-DSC measurements and DSC curves at different heating rates.

From Table 1, we found that the peak temperature of CL-14 was higher than that of HMX, and the heat of decomposition of CL-14 was higher by 4–5 times than that of HMX. The characteristic parameters of thermal decomposition indicated that CL-14 possessed higher

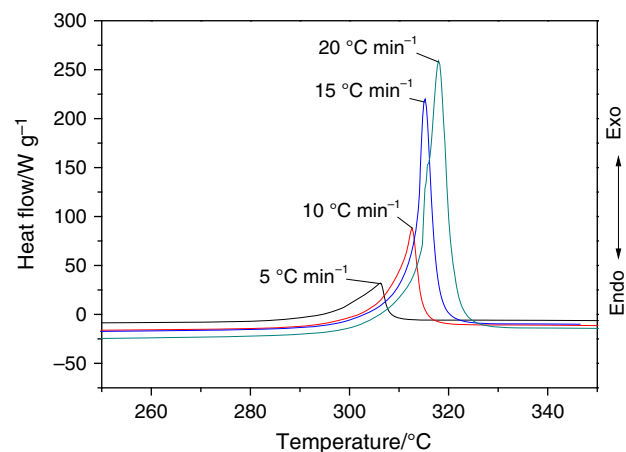


Fig. 2 The effect of heating rate on the DSC curves of CL-14 by DSC instrument

Table 1 Characteristic parameters of thermal decomposition for CL-14 and HMX samples

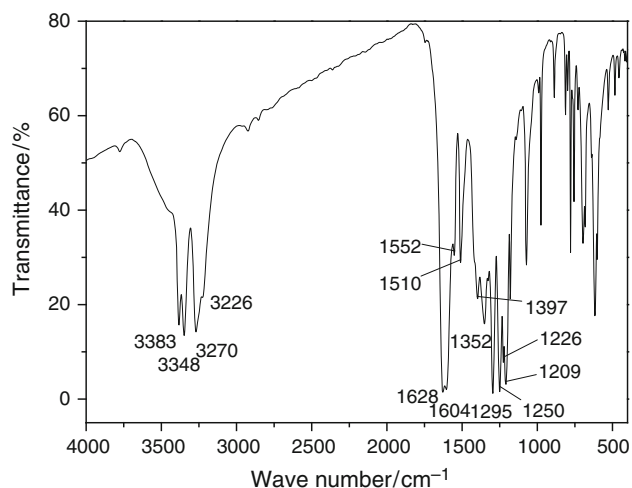
$\beta/$ $^{\circ}\text{C min}^{-1}$	CL-14				HMX [28]	
	$T_0/^{\circ}\text{C}$	$T_p/^{\circ}\text{C}$	$T_f/^{\circ}\text{C}$	$Q_d/\text{J g}^{-1}$	$T_p/^{\circ}\text{C}$	$Q_d/\text{J g}^{-1}$
5	297.2	306.2	308.0	4600.4	278.8	1132.1
10	308.5	312.6	314.8	5128.3	282.1	1281.1
15	313.0	315.2	317.8	5202.5	285.1	1411.7
20	314.6	318.0	321.1	5415.8	287.6	1543.3

β is the heating rate, T_0 is the onset temperature of the decomposition reaction, T_p is the peak temperature in DSC curve, T_f is the end temperature of the thermal decomposition and Q_d is the heat of decomposition

thermal stability than HMX. However, the potential energy of CL-14 was also considerably higher than that of HMX.

Condensed phase compound analysis by RSFT-IR

To investigate the thermal decomposition mechanism of CL-14, the condensed phase products of CL-14 were measured by RSFT-IR at different temperatures. The typical FT-IR spectrum of CL-14 at ambient temperature (before heating) is shown in Fig. 3, and the relationship between infrared absorption frequency and the functional group of the condensed phase of CL-14 is listed in Table 2. We can infer from Fig. 3 and Table 2 that the wave number at 3383, 3348, 3270 and 3226 cm^{-1} may be assigned to $-\text{NH}_2$, whereas the peak at 1628 cm^{-1} may be assigned to the furoxan ring. In addition, peaks at 1552 and 1352 cm^{-1} may be assigned to $-\text{NO}_2$, whereas those at 1604, 1510 and 1397 cm^{-1} may be assigned to the benzene ring. The evident variation in the FT-IR characteristic

**Fig. 3** FT-IR spectrum of condensed phase of CL-14 at ambient temperature

absorption peaks of CL-14 at the range of 140–350 $^{\circ}\text{C}$ is shown in Fig. 4.

As can be seen in Fig. 4, the intensity of the characteristic absorption peaks of $-\text{NH}_2$, furoxan ring, $-\text{NO}_2$ and benzene ring decreased with the increase in temperature, whereas the absorption peaks of CO_2 at 2400 and 2280 cm^{-1} increased as a result of decomposition.

Gaseous product analysis by FT-IR

Gaseous products during the thermal decomposition of CL-14 in the temperature range of 35–380 $^{\circ}\text{C}$ were identified using FT-IR spectra (shown in Fig. 5). Characteristic peaks evidently exist in the frequency ranges of 2359, 2286, 2174 and 1912 cm^{-1} , which correspond to CO_2 , HNCO, CO and NO, respectively. The relationship between infrared absorption frequency and gaseous compounds are listed in Table 3. The FT-IR spectra of CL-14 decomposition gaseous compounds in the temperature range of 235–355 $^{\circ}\text{C}$ are shown in Fig. 6. We can see from Fig. 6 that most of the gaseous products were produced at approximately 300 $^{\circ}\text{C}$. Only one decomposition progress occurs in CL-14, which is in agreement with the study of TG-DSC and DSC measurements.

Gaseous product analysis by MS

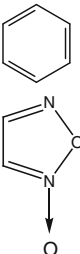
Figure 7 shows the mass spectra of the main gaseous products of CL-14. The figure reveals that the mixtures possess ion current numbers (m/z) of 18, 28, 30, 43 and 44, among which the ion current intensity of $m/z = 30$ is the highest. Based on the literature survey [29–31], several possible species include water ($\text{H}_2\text{O} = 18$), carbon monoxide ($\text{CO} = 28$) or nitrogen ($\text{N}_2 = 28$), nitric oxide ($\text{NO} = 30$), cyanic acid ($\text{HNCO} = 43$) and carbon dioxide ($\text{CO}_2 = 44$). The relative intensity of each pure chemical species obtained by Eq. (1) is summarized in Table 4.

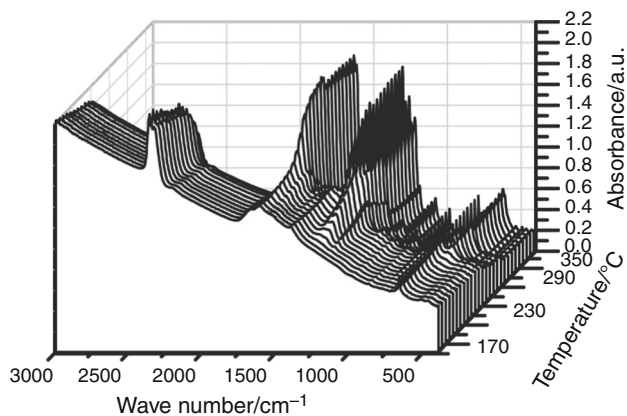
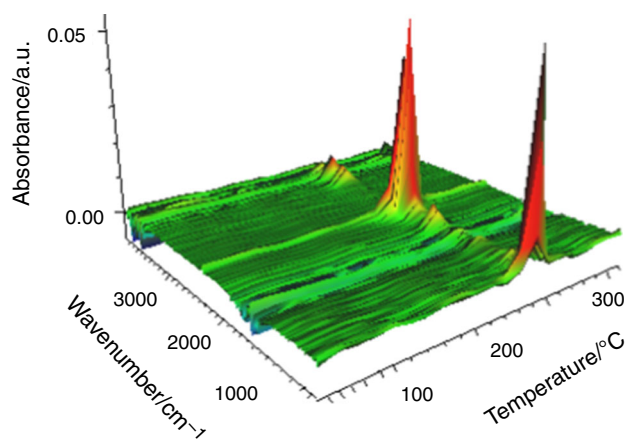
$$r(i) = h(i)/\sum h(i) \quad (1)$$

In the equation, $r(i)$ represents the ratio of the each species with all chemicals, and $h(i)$ represents the height of the m/z peak in the mass spectrum of each species.

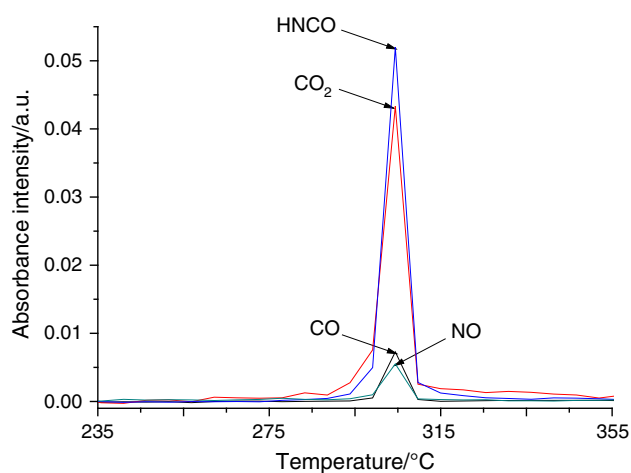
In addition, the onset temperature (T_0), peak temperature (T_p) and end temperature (T_f) detected in the mass spectrum of CL-14 are also listed in Table 4. As can be seen from Table 4, the main gaseous products were NO, CO_2 and H_2O . The first compound produced at the temperature of 267.4 $^{\circ}\text{C}$ by the decomposition of CL-14 was H_2O ($m/z = 18$). This fragment may originate from the concordant reaction, which occurs with the involvement of NH_2 and NO_2 groups. Then, the compound produced CO, N_2 , NO, HNCO and CO_2 at the temperature range of 273.3–299.1 $^{\circ}\text{C}$.

Table 2 The relationship between infrared absorption frequency and functional group of the CL-14 condensed phase

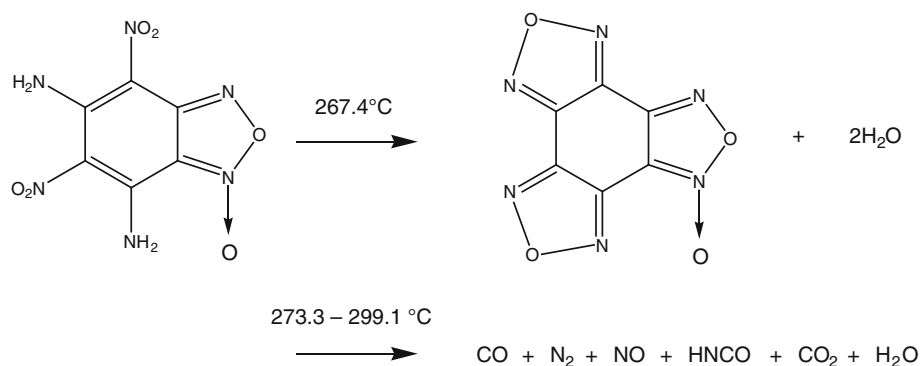
Function groups	Wavenumbers/cm ⁻¹	Comments
C-NH ₂	3383, 3348	ν_{as} NH ₂
	3270, 3226	ν_s NH ₂
	1295, 1250, 1226, 1209	ν C-N
C-NO ₂	1552	ν_{as} NO ₂
	1350	ν_s NO ₂
	1604, 1510	Ring stretching vibration
	1628, 1510, 1397	Ring stretching vibration

**Fig. 4** RSFT-IR characteristic absorption peak intensity of the CL-14 condensed phase at different temperatures**Fig. 5** FT-IR spectra of decomposition gaseous products of CL-14 at different temperatures**Table 3** The relationship between infrared absorption frequency and gaseous products

Wave number/cm ⁻¹	Gaseous products
2359	CO ₂
2286	HNCO
2174	CO
1912	NO

**Fig. 6** FT-IR absorbance intensity of the decomposition gaseous products of CL-14 at different temperatures

We inferred from the analysis of the result of RSFT-IR and TG-DSC-FT-IR-MS that the thermal decomposition process of CL-14 may be explained by the following reaction pathway according to experiments and calculations [32–34].



Nonisothermal decomposition kinetics

To reveal the thermal safety of CL-14, nonisothermal decomposition kinetics was calculated according to DSC data at different heating rates. The parameters of the decomposition kinetics of CL-14 was calculated using multiple heating methods, including the Kissinger method [Eq. (2)] [35] and the Ozawa method [Eq. (3)] [36].

$$\ln\left(\frac{\beta}{T_p^2}\right) = \ln\frac{AR}{E} - \frac{E}{RT_p} \quad (2)$$

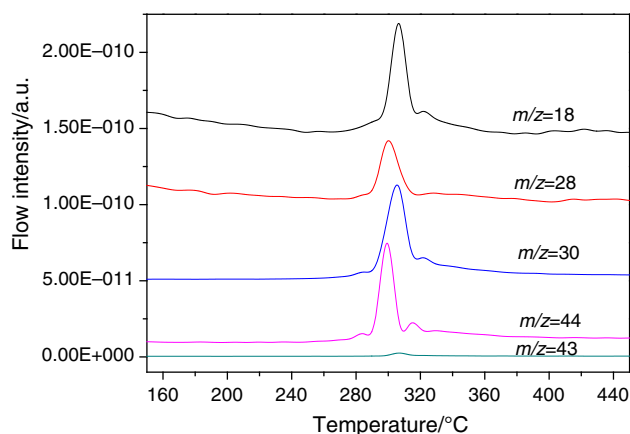


Fig. 7 Ion currents of selected ions representing the main evolved chemical species during thermal decomposition of CL-14

$$\lg \beta = \lg \left[\frac{AE}{RG(\alpha)} \right] - 2.315 - 0.4567 \frac{E}{RT} \quad (3)$$

In these equations, β is the heating rate (K min^{-1}), T_p is the peak temperature in the DSC curve (K), A is the pre-exponential constant, R is the gas constant, E is apparent activation energy (kJ mol^{-1}), α is the conversion degree, $G(\alpha)$ is the integral model function and T is the temperature (K). The kinetic parameter values of the thermal decomposition reaction of CL-14 as obtained by Eqs. (2) and (3) are listed in Table 5. In addition to the kinetic parameters of CL-14, those of ammonium dinitramide (ADN) [37] and 3-nitro-1,2,4-triazol-5-one guanidine salt (GNTO) [38] are also listed in Table 5 for comparison.

As can be seen from Fig. 2 and Table 2, the peak temperature of CL-14 ranged between 306.2 and 318.0 °C. The apparent activation energies of CL-14 were 328.7 and 321.8 kJ mol^{-1} by Kissinger method and the Ozawa method, respectively. The thermal stability of CL-14 was better than those of ADN and GNTO.

Thermal safety

Thermal conductivity

Thermal conductivity (λ) for the decomposition reaction could be calculated using the following equation [39]:

$$\lambda = \frac{3.7287 \times 10^{-5} C_p^{3.0116} \rho^{0.9276}}{T_m^{-0.7652} M^{0.2158}} \quad (4)$$

Table 4 Integrated ion current value of MS spectra and chemical composition of gas mixture

Chemical formula	Compounds name	m/z	$T_0/^\circ\text{C}$	$T_p/^\circ\text{C}$	$T_f/^\circ\text{C}$	Mass/%
H ₂ O	Water	18	267.4	306.5	340.0	24.0
CO/N ₂	Carbon monoxide/nitrogen	28	279.2	300.2	319.9	14.8
NO	Nitric oxide	30	273.3	305.5	333.8	33.4
HNCO	Cyanic acid	43	299.1	299.3	315.2	1.0
CO ₂	Carbon dioxide	44	275.7	306.8	323.8	26.8

Table 5 Kinetic parameters of the thermal decomposition reaction of CL-14 and other energetic materials

Explosive	Kissinger			Ozawa		
	$E/\text{kJ mol}^{-1}$	$\lg(A/\text{s}^{-1})$	r	$E/\text{kJ mol}^{-1}$	$\lg(A/\text{s}^{-1})$	r
CL-14	328.7	27.62	0.9974	321.8	–	0.9976
ADN	169.6	6.31	0.9981	–	–	–
GNT0	262.4	23.71	0.9849	258.0	–	0.9859

In the table, r is the linear correlation coefficient

Table 6 Explosive parameters and comparison of experimental and predicted 50 % drop heights

No.	Explosive	$\lambda \times 10^{-4}/\text{W m}^{-1} \text{K}^{-1}$	$\rho/\text{g cm}^{-3}$	$\lg(A/\text{s}^{-1})$	$Q_d/\text{J g}^{-1}$	$E/\text{kJ mol}^{-1}$	H_{50}/cm		$T_b/^\circ\text{C}$
							Exp.	Predicted	
1	HMX [28]	34.43	1.790	33.80	2764.2	373.70	32	33.40	279.9
2	GNT0 [38]	–	–	23.71	1026.3	262.40	–	–	256.3
3	RDX [29]	10.58	1.660	12.50	2810.4	140.00	26	20.10	
4	CL-14	35.20	1.932	27.62	5086.3	328.70		39.79	307.9

where C_p is the specific heat capacity ($\text{J g}^{-1} \text{K}^{-1}$), ρ is the density of CL-14 (g cm^{-3}), T_m is the melting point (K) and M is the molecular weight of CL-14.

By substituting the values of $C_p = 1.14 \text{ J g}^{-1} \text{K}^{-1}$, $T_m = 489.5 \text{ K}$, $M = 256$ and $\rho = 1.932 \text{ g cm}^{-3}$ [27] into Eq. (4), the value of λ ($\lambda = 35.2 \times 10^{-4} \text{ W m}^{-1} \text{K}^{-1}$) was obtained.

Self-accelerating decomposition temperature

The value (T_{e0}) of the onset temperature (T_e) corresponding to $\beta \rightarrow 0$ was obtained by Eq. (5), and the self-accelerating decomposition temperature (T_{SADT}) obtained by Eq. (6) was $282.0 \text{ }^\circ\text{C}$ for CL-14 [40]:

$$T_{ei} = T_{e0} + b\beta_i + c\beta_i^2 + d\beta_i^3 \quad i = 1, 2, 3, 4 \quad (5)$$

where b , c and d are coefficients, and β is the heating rate (K min^{-1}).

$$T_{\text{SADT}} = T_{e0} \quad (6)$$

Critical temperature of thermal explosion

The critical temperature of thermal explosion (T_b) is an important parameter for energetic materials to ensure safe storage and operations when used in propellants, explosives and pyrotechnics. Equation (7) was used to obtain the value of T_b for CL-14 [41, 42].

$$T_b = \frac{E_0 - \sqrt{E_0^2 - 4E_0RT_{e0}}}{2R} \quad (7)$$

where E_0 is apparent activation energy obtained by Ozawa method (kJ mol^{-1}), R is the gas constant ($\text{J mol}^{-1} \text{K}^{-1}$) and T_{e0} is the onset temperature (K).

By substituting the values of $E_0 = 321.8 \text{ kJ mol}^{-1}$, $R = 8.314 \text{ J mol}^{-1} \text{K}^{-1}$ and $T_{e0} = 572.2 \text{ K}$ into Eq. (7), we obtain the value of T_b of $307.9 \text{ }^\circ\text{C}$.

Characteristic drop height of impact sensitivity

The impact sensitivity is an important parameter for evaluating the security and reliability of EMs and can be characterized by 50 % drop height (H_{50}). The characteristic drop height for impact sensitivity (H_{50}) for the decomposition reaction can be calculated using Eq. (8) [43]:

$$\frac{1}{2}n \lg H_{50} + \lg \sqrt{\frac{\lambda}{A\rho Q_d}} + D_3 + \frac{0.02612E}{T_1 + D_2 H_{50}^n} = 0 \quad (8)$$

where n , D_2 and D_3 are parameters of the correlation, λ is thermal conductivity ($\text{W m}^{-1}\text{K}^{-1}$), A is the pre-exponential constant, ρ is the density of CL-14 (g cm^{-3}), Q_d is the heat of decomposition (J g^{-1}) and E is apparent activation energy obtained by Kissinger method (kJ mol^{-1}).

The corresponding values of $n = 0.564623$, $D_2 = 33.8765$ and $D_3 = -0.347174$ are obtained in the literature [44]. By substituting the values of $\lambda = 35.2 \times 10^{-4} \text{ W m}^{-1} \text{K}^{-1}$, $\rho = 1.932 \text{ g cm}^{-3}$, $A = 10^{27.62} \text{ s}^{-1}$, $Q_d = 5086.3 \text{ J g}^{-1}$ and $E = 328.7 \text{ kJ mol}^{-1}$ into Eq. (8), the H_{50} value of 39.79 cm was obtained. The characteristic drop height of impact sensitivity and the critical temperature of thermal explosion of CL-14, GNT0, HMX and RDX are

listed in Table 3 to compare the thermal stability of energetic materials.

As can be seen from Table 3, the order of critical explosion temperature is $T_{b(\text{CL-14})} = 307.9\text{ }^\circ\text{C} > T_{b(\text{HMX})} = 279.9\text{ }^\circ\text{C} > T_{b(\text{GNTO})} = 256.3\text{ }^\circ\text{C}$, whereas the order of the characteristic drop height of impact sensitivity is $H_{50(\text{CL-14})} = 39.79\text{ cm} > H_{50(\text{HMX})} = 33.4\text{ cm} > H_{50(\text{RDX})} = 20.1\text{ cm}$. The results indicated that CL-14 possesses an insensitive nature and better thermal stability in comparison with HMX, GNTO and RDX (Table 6).

Conclusions

The thermal decomposition of CL-14 was examined in terms of its evolved gases and condensed products during linear heating. Using RSFT-IR and TG-DSC-FT-IR-MS, species of evolved gases and condensed products were identified. Mass spectrometer and FT-IR analysis confirmed that H_2O , CO , N_2 , NO , HNCO and CO_2 are the gaseous decomposition products. The decomposition progress was proposed according to the results of the examination by RSFT-IR and TG-DSC-FT-IR-MS, as well as results from the literature. The nonisothermal decomposition kinetics of CL-14 was calculated according to DSC data at different heating rates. E and A were obtained by Kissinger and Ozawa methods. The thermal stability parameters of CL-14 are as follows: $T_{\text{SADT}} = 282.0\text{ }^\circ\text{C}$, $T_b = 307.9\text{ }^\circ\text{C}$ and $H_{50} = 39.79\text{ cm}$. Results indicated that CL-14 possesses an insensitive nature with better thermal stability in comparison with HMX, GNTO and RDX.

References

- Šarlauskas J, Anusevičius Z, Misiunas A. Benzofuroxan (benzo [1,2-c] 1,2,5-oxadiazole N-oxide) derivatives as potential energetic materials: studies on their synthesis and properties. *Cent Eur J Energ Mater*. 2012;9:365–86.
- Nair U, Asthana S, Rao AS, Gandhe B. *Adv High Energy Mater Def Sci J*. 2010;60:137–51.
- Pepkin V, Korsunskii B, Matyushin YN. Explosive properties of furoxanes. *Combust Explos Shock Waves*. 2008;44:110–4.
- Türker L, Variş S. A review of polycyclic aromatic energetic materials. *Polycyclic Aromat Compd*. 2009;29:228–66.
- Zhang C. Investigations of correlation between nitro group charges and C-nitro bond strength, and amino group effects on C-nitro bonds in planar conjugated molecules. *Chem Phys*. 2006;324:547–55.
- Zhang C. Computational investigation of the detonation properties of furazans and furoxans. *J Mol Struct*. 2006;765:77–83.
- J-s Li. Relationships for the impact sensitivities of energetic C-nitro compounds based on bond dissociation energy. *J Phys Chem B*. 2010;114:2198–202.
- Wang J, Li J, Liang Q, Huang Y, Dong H. A novel insensitive high explosive 3,4-bis (aminofurazano) furoxan. *Propellants Explos Pyrotech*. 2008;33:347–52.
- Bogdanova YA, Gubin S, Korsunskii B, Pepkin V. Detonation characteristics of powerful insensitive explosives. *Combust Explos Shock Waves*. 2009;45:738–43.
- Badgajar D, Talawar M, Asthana S, Mahulikar P. Advances in science and technology of modern energetic materials: an overview. *J Hazard Mater*. 2008;151:289–305.
- He C, Zhang J, Parrish DA, Jean'ne MS. 4-Chloro-3,5-dinitropyrazole: a precursor for promising insensitive energetic compounds. *J Mater Chem A*. 2013;1:2863–8.
- Sikder A, Sinha R, Gandhe B. Cost-effective synthesis of 5,7-diamino-4,6-dinitrobenzofuroxan (CL-14) and its evaluation in plastic bonded explosives. *J Hazard Mater*. 2003;102:137–45.
- Norris WP. Insensitive high density explosive, in, US, 5039812. 1991-08-13.
- Dong Y, Liu ZL. Effect of refining on the properties of 5,7-diamino-4,6-dinitrobenzofuroxan. *Chin J Energ Mater*. 2013;21:706–10.
- Dong Y, Liu ZL, Su Q, Hao YG. Preparation of 5,7-diamino-4,6-dinitrobenzofuroxan. *Explos Mater*. 2013;42:10–3.
- Sikder AK, Pawar S, Sikder N. Synthesis, characterisation, thermal and explosive properties of 4,6-dinitrobenzofuroxan salts. *J Hazard Mater*. 2002;90:221–7.
- Sikder A, Sikder N. A review of advanced high performance, insensitive and thermally stable energetic materials emerging for military and space applications. *J Hazard Mater*. 2004;112:1–15.
- Zhang W, Luo Y, Li J, Li X. Thermal decomposition of aminonitrobenzodifuroxan. *Propellants Explos Pyrotech*. 2008;33:177–81.
- Liu Y, Gong X, Wang L, Wang G, Xiao H. Substituent effects on the properties related to detonation performance and sensitivity for 2,2',4,4',6,6'-hexanitroazobenzene derivatives. *J Phys Chem A*. 2011;115:1754–62.
- Saikia A, Sivabalan R, Polke B, Gore G, Singh A, Subhananda Rao A, Sikder A A. Synthesis and characterization of 3, 6-bis (1H-1,2,3,4-tetrazol-5-ylamino)-1,2,4,5-tetrazine (BTATz): novel high-nitrogen content insensitive high energy material. *J Hazard Mater*. 2009;170:306–13.
- Zulumyan N, Mirgorodski A, Isahakyan A, Beglaryan H. The mechanism of decomposition of serpentines from peridotites on heating. *J Therm Anal Calorim*. 2014;115:1003–12.
- Zhang GZ, Zheng HC, Xiang X. Thermal decomposition and kinetics studies on the 2,2-dinitropropyl acrylate–styrene copolymer and 2,2-dinitropropyl acrylate–vinyl acetate copolymer. *J Therm Anal Calorim*. 2013;111:1039–44.
- Georgieva V, Zvezdova D, Vlaev L. Non-isothermal kinetics of thermal degradation of chitin. *J Therm Anal Calorim*. 2013;111:763–71.
- Zhang JQ, Gao HX, Ji TZ, Xu KZ, Hu RZ. Non-isothermal decomposition kinetics, heat capacity and thermal safety of 37.2/44/16/2.2/0.2/0.4-GAP/CL-20/Al/N-100/PCA/auxiliaries mixture. *J Hazard Mater*. 2011;193:183–7.
- Gaoka P, Kowalonek J, Kaczmarek H. Thermogravimetric analysis of thermal stability of poly(methyl methacrylate) films modified with photoinitiators. *J Therm Anal Calorim*. 2014;115:1387–94.
- Guo S, Wan W, Chen C, Chen WH. Thermal decomposition kinetic evaluation and its thermal hazards prediction of AIBN. *J Therm Anal Calorim*. 2013;113:1169–76.
- Wang BZ, Huo H, Li JZ, Fan XZ, Liu Q. Synthesis and characterization of 4,6-dinitro-5,7-diamino benzofuroxan (CL-14). *Chin J Organ Chem*. 2011;31:132–5.

28. Tang Z, Yang L, Qiao XJ, Zhang TL, Yu WF. On thermal decomposition kinetics and thermal safety of HMX. *Chin J Energ Mater.* 2011;19:396–400.
29. Zhu YL, Huang H, Ren H, Jiao QJ. Influence of aluminum particle size on thermal decomposition of RDX. *J Energ Mater.* 2013;31:178–91.
30. Kwon E, Castaldi MJ. Fundamental understanding of the thermal degradation mechanisms of waste tires and their air pollutant generation in a N₂ atmosphere. *Environ Sci Technol.* 2009;43:5996–6002.
31. Zhu Y, Xiao Z, Jiao Q, Ren H, Huang H. Effects of aluminum on thermal decomposition of hexogen/ammonium perchlorate. *Chem Res Chin Univ.* 2014;30:666–71.
32. Matveev VG, Dubikhin VV, Nazin GM. Concordant mechanism for gas-phase decomposition of nitro compounds. *Bull Acad Sci USSR Div Chem Sci.* 1978;27:411–3.
33. Bell A, Eadie E, Read R, Skelton B, White A. 2,2',4,4',6,6'-Hexanitrobiphenyl-3,3',5,5'-tetramine: synthesis and comparison of physicochemical properties with those of other amino nitro biphenyls. *Aust J Chem.* 1987;40:175–86.
34. Rogers RN, Janney JL, Ebinger MH. Kinetic-isotope effects in thermal explosions. *Thermochim Acta.* 1982;59:287–98.
35. Kissinger HE. Reaction kinetics in differential thermal analysis. *Anal Chem.* 1957;29:1702–6.
36. Ozawa T. A new method of analyzing thermogravimetric data. *Bull Chem Soc Jpn.* 1965;38:1881–6.
37. Zhai JX, Yang RJ, Li XD. Combustion and thermal decomposition of ammonium dinitramide. *Chin J Explos Propellants.* 2005;28:83–6.
38. Xu KZ, Zhao FQ, Yang R, Ren YH, Ma HX, Song JR. Non isothermal decomposition kinetics, specific heat capacity and adiabatic time-to-explosion of GNTO. *J Solid Rocket Technol.* 2009;32:74–8.
39. Hu RZ, Zhao FQ, Gao HX, Ma HX, Zhang H, Xu KZ, Zhao HA, Yao EG. The thermal safety and a density functional theoretical study on bis(2,2,2-trinitroethyl)-nitramine (BTNNA). *Chin J Explos Propellants.* 2013;36:9–16.
40. Tseng JM, Lin CP, Huang ST, Hsu J. Kinetic and safety parameters analysis for 1,1,-di-(tert-butylperoxy)-3,3,5-trimethylcyclohexane in isothermal and non-isothermal conditions. *J Hazard Mater.* 2011;192:1427–36.
41. Sovizi M, Hajimirsadeghi S, Naderizadeh B. Effect of particle size on thermal decomposition of nitrocellulose. *J Hazard Mater.* 2009;168:1134–9.
42. Yi JH, Zhao FQ, Gao HX, Xu SY, Wang MC, Hu RZ. Preparation, characterization, non-isothermal reaction kinetics, thermodynamic properties, and safety performances of high nitrogen compound: hydrazine 3-nitro-1,2,4-triazol-5-one complex. *J Hazard Mater.* 2008;153:261–8.
43. Yi JH, Zhao FQ, Wang BZ, Liu Q, Zhou C, Hu RZ, Ren YH, Xu SY, Xu KZ, Ren XN. Thermal behaviors, nonisothermal decomposition reaction kinetics, thermal safety and burning rates of BTATz-CMDB propellant. *J Hazard Mater.* 2010;181:432–9.
44. Hu RZ, Zhao FQ, Gao HX, Zhang H, Zhao HA, Wang X, Zhang X, Feng Y, Ma H. The estimation of characteristic drop heights of impact sensitivity for polymer bonded explosives JH-94 and JO-96. *Chin J Energ Mater.* 2009;17:251.